

pubs.acs.org/JPCC Article

Intersystem Crossing in Tetrapyrrolic Macrocycles. A First-Principles Analysis

Srijana Bhandari, Sunandan Sarkar, Alexander Schubert, Atsushi Yamada, Jameson Payne, Marcin Ptaszek, Eitan Geva, and Barry D. Dunietz*



Cite This: J. Phys. Chem. C 2021, 125, 13493-13500



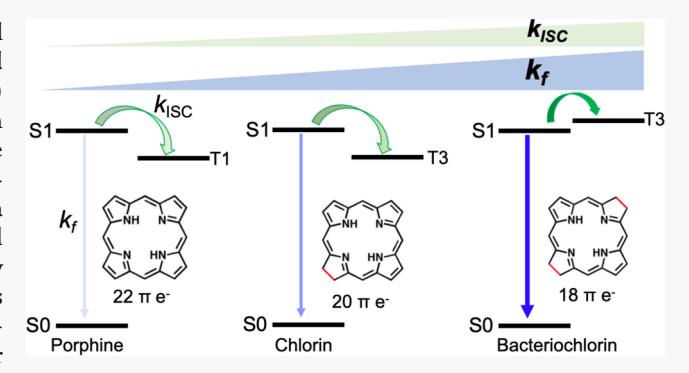
ACCESS

III Metrics & More

Article Recommendations

s Supporting Information

ABSTRACT: We analyze reported trends of the photophysical properties in a series of tetrapyrrolic macrocycles with varied saturation level. We compare rates of intersystem crossing (ISC) and fluorescence upon photoabsorption in porphine (P), chlorin (CH), and bacteriochlorin (BC). CH and BC result from single hydrogenation and double hydrogenation of P, respectively. A first-principles time-dependent density functional theory based on a novel framework is used to implement a quantum-mechanical Fermi's golden rule (FGR) rate theory. We employ the recently developed screened range-separated hybrid (SRSH) functionals and a polarizable continuum model (PCM) achieving a polarization-consistent description of the embedded molecular electronic structure. We find, in agreement with the measurements,



an increase of the ISC rate upon hydrogenation originating in an increase of the spin—orbit coupling (SOC). This trend is traced back to the overlap of attachment and detachment densities of the relevant singlet and triplet states. Simultaneously, we find an increase in the fluorescence rate competing with the ISC, which, overall, results in a lower ISC yield with increasing degree of hydrogenation despite the increased SOC. Crucially, both the quantum mechanical perspective in the FGR theory and the polarization consistent formulation achieved by the screened RSH used in the DFT calculations are required for achieving predictive quality in the calculated rates.

INTRODUCTION

Photosensitization involving triplet excited states in organic molecules has been widely addressed in the context of reactive oxygen species (ROS), photodynamic therapy (PDT), 1,2 phosphorescence,³ photocatalysis,¹ and singlet-triplet upconversion.4 Triplet states in organic molecules can be generated upon photoexcitation through the formally forbidden intersystem crossing (ISC), S1 \rightarrow Tn (S1 denotes the lowest singlet excited state, and Tn denotes the nth triplet excited state) that is enabled by spin-orbit coupling (SOC).5 Typically, SOC in organic materials is relatively weak.5 However, some exceptions of organic molecules with larger SOC presenting high quantum yields of ISC have been reported.^{6,7} SOC values larger than 0.2 cm⁻¹ are generally accepted as significant enough to induce ISC. 8-10 For example, in derivatives of boron-dipyrromethene (BODIPY) metal-free organic materials that are associated with large quantum yield of triplet states, the calculated SOCs range between 0.2 and 3.2 cm^{-1.6} Relatively strong SOC can be achieved through heavy atom effects, where the organic materials are functionalized by a heavy nonorganic element, e.g., Br, I, S, or a transition metal.^{1,5,11} An example of increased SOC with heavy atom effect is seen in zinc ligated chlorophyll of 390 cm⁻¹.

Significant ISC has been reported also for tetrapyrrolic macrocycles^{2,13} including porphine (P),^{2,14} chlorin (CH),¹³ and bacteriochlorin (BC).¹⁵ On the other hand, competing relaxation processes that deactivate S1, for example, fluorescence, tend to be associated with larger rate constants for CH and BC⁵ ($k_f > 10^8 \text{ s}^{-1}$).

Porphyrins are fully conjugated tetrapyrrolic macrocyclic compounds, where CH and BC result from single and double hydrogenation of P, respectively. The partially hydrogenated CH and BC systems retain a conjugated ring character. The molecular structures of P, CH, and BC are presented in Figure 1, where hydrogenation sites are highlighted. CH and BC are the key photosynthetic pigments in chlorophyll and bacteriochlorophyll photosystems exhibiting deep red or near-infrared (IR) fluorescence. These pigments are widely used as

Received: May 5, 2021 **Revised:** May 22, 2021 **Published:** June 10, 2021











Figure 1. Porphine (P), chlorin (CH), and bacteriochlorin (BC) molecular structures. CH results from single hydrogenation of the P conjugated system, and BC is made through double hydrogenation. The hydrogenated bonds are highlighted by red color. Atomic coordinates are provided in the Supporting Information.

fluorescent probes for in vivo imaging, ^{6,14,16–26} phototherapy, ² and solar energy conversion applications. ^{27,28}

Measured spectral data find that the lowest absorption peak is red-shifted upon hydrogenation as we proceed in the series P < CH < BC. Also well-known is the trend of increasing absorption and emission intensities in this series, 29 causing P to have the slowest fluorescence 13,15 as dictated by the Einstein coefficients that are proportional to the spectral intensity following the Strickler–Berg relation. In Figure 2, we

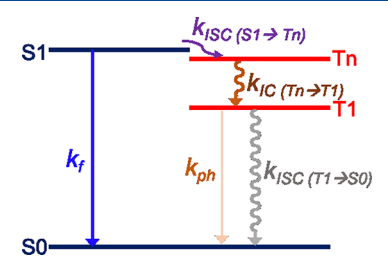


Figure 2. Jablonski diagram highlighting the electronic states involved in the deactivation of S1 excited state. S1 deactivation can proceed directly through fluorescence or by ISC to a triplet excited state (Tn) followed by internal conversation (IC) to the lowest triplet state, T1, as dictated by Kasha's rules.

represent the two radiative relaxation processes originating at the lowest excited singlet state, S1. To the left of the figure, we follow the fluorescence of direct relaxation to the ground state. To the right we find phosphorescence (ph) that amounts to relaxation from the lowest triplet state, T1. 32 The T1 population stems from ISC to a Tn state and subsequent internal conversion (IC).

The ISC process appears to present a complex relationship at the molecular level, where the rates, $k_{\rm ISC}$, are found to form the following weak trend in the hydrogenated series: P < CH < BC, 13,15 whereas the quantum yield, $\Phi_{\rm ISC}$, appears to decrease significantly. 33 The $\Phi_{\rm ISC}$ is also known to be strongly affected by the competing fluorescence rate that increases within the series with the extinction coefficient of the longest wavelength absorption band.

To understand these trends, we analyze the relationships of the ring saturation and the formation of T1 in the tetrapyrrolic macrocycles. We analyze computationally the spectral properties and photorelaxation of the molecular series. We explain the observed photoactivity of these molecules and, in particular, address the generation of triplet excited states. We investigate the structure—function relationships that determine the SOC in these molecules and compare the rates of ISC to those of competing fluorescence that also deactivates the S1 states.

We employ the recently developed and well benchmarked polarization-consistent SRSH-PCM^{34–36} scheme to calculate

the potential energy surfaces used to obtain ISC rate constants at a fully quantum mechanical level of theory. The SRSH-PCM scheme is a relatively novel framework that was shown to achieve unique insight for several related pigments.^{37–39} Importantly, we follow our well established protocol based on Fermi's golden rule (FGR) rate theory that goes beyond the semiclassical limit of the widely employed Marcus theory.^{40–43} In earlier studies, FGR ISC rates in porphyrinic rings have been found to be significantly larger than the ones obtained using approximated expressions.⁴⁴

■ COMPUTATIONAL APPROACH

Electronic structure calculations are performed using the time-dependent density functional theory (TDDFT) of the screened RSH (SRSH)³⁴ functional based on PBEh.^{45,46} The SRSH range-separation parameter is tuned following the J2 scheme.⁴⁷ (The tuned parameters for P, CH, and BC are 0.227, 0.228, and 0.230 bohr⁻¹, respectively.) Both RSH and the SRSH DFT calculations are employed within the polarizable continuum model (PCM)^{48,49} to represent the dielectric environment. In the SRSH framework, the XC functional takes the following form:

$$\begin{split} E_{\text{XC}}^{\text{SRSH}} &= \alpha E_{F_{\text{X}}}^{\text{SR}} + (1 - \alpha) E_{\text{D}F_{\text{X}}}^{\text{SR}} + (\alpha + \beta) E_{F_{\text{X}}}^{\text{LR}} \\ &+ (1 - \alpha - \beta) E_{\text{D}F_{\text{Y}}}^{\text{LR}} + E_{\text{D}F_{\text{C}}}, \end{split}$$

where SR and LR indicate short-range and long-range terms, X and C denote exchange and correlation, and F and DF indicate Fock exchange and the semilocal density functional, respectively. Importantly, in SRSH-PCM calculations, the β parameter is reset such that $\beta = 1/\epsilon - \alpha$. Here ϵ corresponds to the scalar static dielectric constant of the environment that is also invoked within the PCM, and α is kept at the default value of the RSH functional. Importantly, SRSH-PCM achieves physically meaningful frontier orbitals of the molecular system in a condensed phase (solution or crystal),³⁴ a property that is crucial for the quality of the calculated excited states.³⁵ More recently, we have shown that the SRSH-PCM scheme achieves accurate triplet excitation energies as well.³⁶ In this study we address the simplest (unsubstituted) derivatives of the tetrapyrrolic macrocycles, P, CH, and BC, shown above in Figure 1 solvated in toluene where the static and the optical room temperature dielectric constants 2.38⁵⁰ and 2.24⁵¹ are used in the PCM calculations.

Excited states are obtained using the Tamm–Dancoff approximation (TDA)⁵² and the full TDDFT for comparison. Absorption energies are calculated using SRSH-PCM at the ground state optimized geometry. The emission energy shift is calculated using SRSH-PCM at the geometry of the respective excited state optimized by TDDFT with RSH-PCM.

All calculations including the geometry optimizations are performed using the 6-311+G** basis set, except for the SOC calculations, which are performed employing the one-electron Breit—Pauli Hamiltonian⁵³ at the excited state optimized geometry and the 6-311G** basis set. Q-Chem 4⁵⁴ was used to implement most of the electronic structure calculations, while Gaussian⁵⁵ was used to calculate the normal modes needed for the ISC rate evaluation.

The FGR rate constants are given by 56

$$\begin{split} k_{\rm ISC}^{\rm FGR} &= \frac{|V_{{\rm T}n,{\rm S}1}^{\rm SOC}|^2}{\hbar^2} {\rm e}^{-\sum_{\alpha} S_{\alpha}(2n_{\alpha}+1)} \\ &\times \int_{-\infty}^{\infty} {\rm d}t \, \exp\biggl\{ -\frac{t^2}{\tau^2} - \frac{i}{\hbar} \Delta E t \\ &+ \sum_{\alpha} S_{\alpha} [(n_{\alpha}+1) {\rm e}^{-i\omega_{\alpha}t} + n_{\alpha} {\rm e}^{i\omega_{\alpha}t}] \biggr\}. \end{split} \tag{1}$$

Here, $V_{{\rm T}n,{\rm S1}}^{\rm SOC}$ is the SOC constant, $\{\omega_{\alpha}\}$ are the normal modes frequencies, $\{S_{\alpha}\}$ are the Huang–Rhys factors (HRFs), and $n_{\alpha} = \left(\exp\left\{\frac{\hbar\omega_{\alpha}}{k_{\rm B}T}\right\} - 1\right)^{-1}$ are the normal modes thermal

occupancies. The total SOC values are due to combining the contributions from the three quantum triplet states, where in all the cases the SOC contributions from $m_s = 1$ and -1 are nearly vanishing. For all three cases, we use normal modes calculated at singlet ground state geometry in vacuum. The corresponding reorganization energy within the harmonic approximation is given by $\lambda = \sum_{\alpha} \hbar \omega_{\alpha} S_{\alpha}^{40,57}$ The window function $\exp(-t^2/\tau^2)$ was introduced to suppress erroneous recurrences at large times. A value of $\tau = 12.5$ fs was found for P to be sufficiently large to achieve convergence (see the Supporting Information, Figure S4) and was employed for all three molecules. ΔE is the energy difference between the singlet and triplet optimized excited states. Following the high temperature and short time limits, the semiclassical Marcus rate constant can be obtained from the FGR expression: $^{58-61}$

$$k_{\rm ISC}^{\rm M} = \frac{|V_{\rm Tn,S1}^{\rm SOC}|^2}{\hbar} \sqrt{\frac{\pi}{k_{\rm B}T\lambda}} \exp\left(-\frac{(\Delta E - \lambda)^2}{4k_{\rm B}T\lambda}\right)$$
(2)

The fluorescence rate constant, $k_{\rm p}$ is determined by the spectral intensity³⁰ as reflected by the transition dipole moment of the excited state and can be expressed by the oscillator strength (OS) of the excited state and the absorption and emission frequencies, $\nu_{\rm abs}$ and $\nu_{\rm em}$. A simplified and widely used form for $k_{\rm f}$ is given by 31,62

$$k_{\rm f} = 0.6671 \text{ cm}^2 \text{ s}^{-1} \frac{\nu_{\rm em}^3}{\nu_{\rm abs}} n^2 f$$
 (3)

Here n=1.496 is the refractive index of the solvent, toluene, and the OS is denoted by f. ISC and fluorescence rates, $k_{\rm ISC}$ and $k_{\rm f}$, of the molecular series are evaluated and compared to measured values in toluene where available.

■ RESULTS AND DISCUSSION

We start by considering the excitations in toluene at the ground state geometry that affect the absorption spectra. The calculated excited states energies and OSs are listed in Table 1. Importantly the calculated excitations reproduce the observed trend, 14,15,22 where the spectral intensity increases in the series, while the spectral peak is red-shifted in the series upon hydrogenation, P < CH < BC. The calculated singlet excited state energies for all three cases are higher than the measured spectral peak by about 0.3 eV, in agreement with earlier reported trends based on TDDFT values of related systems. $^{63-67}$ We also note that the TDA energies are only slightly larger by less than 0.1 eV in comparison to the full TDDFT energies for P and CH and by about 0.2 eV for the BC case. (See the values listed in the Supporting Information,

Table 1. Excitation Energies Calculated at the Ground State Geometry Compared to Measured Spectral Peaks in the Absorption Spectra (eV)^a

molecule	exp. ^b	calc. ^c	em.		
P	$2.01^{14} (1.95)$	2.37 (0.0001)	2.35(0.0002)		
СН	$1.96^{22} (1.94)$	2.35 (0.18)	2.31(0.22)		
BC	$1.74^{15} (1.70)$	2.13 (0.56)	2.10(0.57)		

^aThe emission energies are obtained at RSH optimized S1 geometry. OSs are provided in the parentheses. ^bMeasured absorption energies of unsubstituted macrocycles in toluene, PEGylated (polyethylene glycol conjugated) forms in DMF¹³ noted in parentheses. ^cTDA and TDDFT energies are compared in the Supporting Information, Table S1.

Table S1). Similar agreement was reported for extended- π conjugated systems.⁶⁷

The observed red shift in the spectral peak and increase of the spectral intensity can be explained by considering the frontier and next to frontier molecular orbitals (MOs). The highest occupied MO (HOMO), next-HOMO (HOMO-1), lowest unoccupied MO (LUMO), and next LUMO (LUMO +1) energies and densities calculated at the ground state geometry are shown in Figure 3. For completeness, orbital

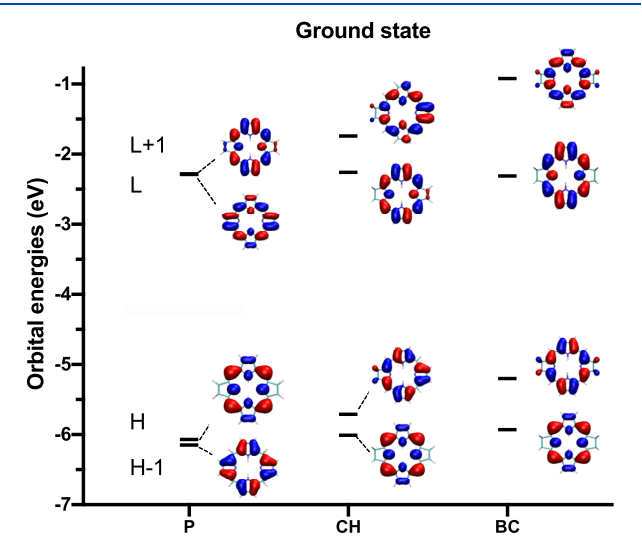


Figure 3. Orbital diagrams at the ground state geometry.

diagrams at the optimized excited singlet state and triplet state geometries are provided in the Supporting Information, Figure S1. The quasi-degeneracies of the HOMO and HOMO—1 and between the LUMO and LUMO+1 observed in P are lifted in CH and BC. The energy splitting of the occupied frontier orbitals increases from 0.08 eV in P to 0.11 and 0.35 eV in CH and BC, respectively. We consider next the low lying electronic excited states that involve these frontier orbitals and analyze the resulting optical trend.

The solvated key excitation energies including the singlet (S1) and the triplet states (Tn) at the S1 optimized geometry are provided in Figure 4. In agreement with the well-known Gouterman model for porphyrins, ^{24,68} the low lying excitations are due to one electron promotions within the frontier molecular orbitals, HOMO-1, HOMO, LUMO, and LUMO +1. The key orbital transitions and amplitudes of the S1-Tn

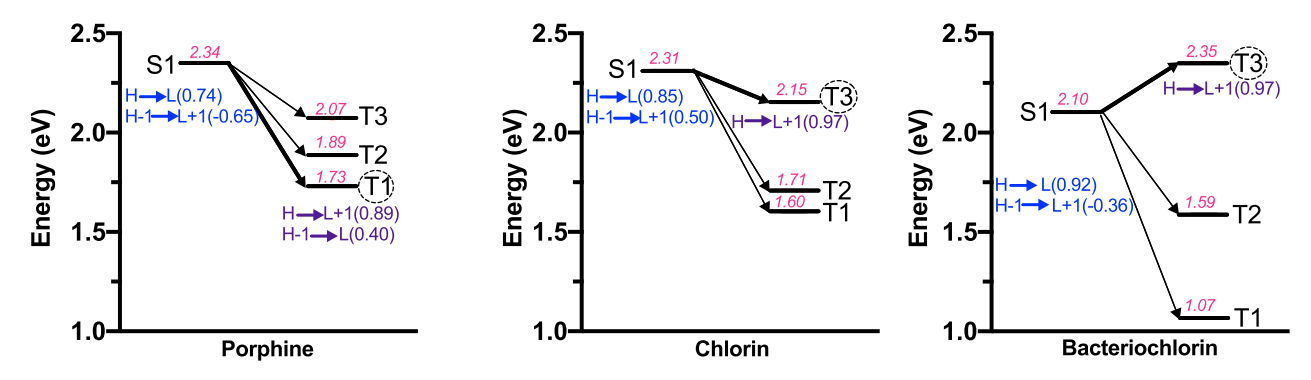


Figure 4. SRSH-PCM vertical singlet and triplet excitation energies calculated in toluene at the RSH-level-optimized S1 geometry. The main orbital transitions for S1 and Tn states are provided respectively in blue and purple color. The width of the transition arrow reflects the relative strength of SOC. The most relevant Tn state for the ISC is highlighted by a circle for each system.

Table 2. Singlet (S1) to Triplet (Tn) Excited State Transitions at S1-Optimized Geometry^a

	P			CH			BC	
$V_{\mathrm{T1,S1}}^{\mathrm{SOC}}$	ΔE	λ	$V_{ m T3,S1}^{ m SOC}$	ΔE	λ	$V_{\mathrm{T3,S1}}^{\mathrm{SOC}}$	ΔE	λ
0.48	-0.74	0.18	0.68	-0.28	0.05	1.09	0.10	0.07

"SOC in cm⁻¹, the energy difference ΔE (eV), and the reorganization energies λ (eV). The relevant transitions are identified based on the strongest SOC between the S1 and Tn states (n = 1 for P and 3 for CH and BC).

states are also indicated in the figure, where a more complete listing is provided in the Supporting Information, Table S2.

Due to the orbital degeneracy for P noted above in Figure 3, the two orbital transitions, HOMO \rightarrow LUMO and HOMO-1 → LUMO+1, have similar coefficients in the expansion forming the low lying excited state.^{69,70} Furthermore, due to the orbital symmetries the resulting transition dipole moments (TDMs) of either individual transitions are of opposite sign resulting in near cancellation of the excited state TDM and therefore of a vanishingly small OS of S1 in P. In the CH and BC cases the lifting of the orbital energy degeneracy leads to different coefficients of the two orbital transitions forming S1. Consequently, the mutual cancellation of the individual TDMs is decreased significantly affecting the overall TDM for the excited state. Indeed, the S1 OS increases in CH and further in BC;⁷⁰ see Table 1. Accordingly, S1 in CH and BC includes a HOMO → LUMO contribution of over 70% and one over 80% (corresponds to 0.85 and 0.92 coefficients).

The parameters determining the intersystem crossing rate, $k_{\rm ISC}$, are the S1 to Tn energy difference, ΔE , the reorganization energy, λ , and the S1–Tn SOC constant, $V_{\rm Tn,S1}^{\rm SOC}$. The parameters calculated at the S1-optimized geometry along with the most relevant triplet state (associated with the largest SOC and rate constant) are listed in Table 2. Also indicated in Figure 4 are the S1–Tn coupling strengths, where the relative strength is highlighted by the line width. The triplet states of the highest SOC to the S1 state are T1 for P and T3 for CH and BC, which are highlighted in Figure 4.

We find that the SOCs do not depend strongly on the geometry. SOC values obtained at other geometries are provided in the Supporting Information, Table S3, where in all the cases they remain in close agreement across the different geometries. For completeness, we also present the SOC involving the three lowest triplet states for the three systems in the Supporting Information, Table S4, where for P only the coupling to T1 is essentially nonvanishing, and for CH and BC the coupling to T3 is by a factor of 5 and 2 larger, respectively, than the next SOC value.

The SRSH singlet-triplet gap between the lowest excited states, Δ S1T1, at the S1 geometry are 0.61, 0.71 and 1.03 eV for P, CH and BC, respectively (see Figure 4). For comparison, an averaged difference obtained for several chlorophylls was recently reported to be 0.55 eV. Similar values of Δ S1T1 have been obtained for a series of synthetic bacteriochlorins by Holten and co-workers.²⁶ For P and CH, the ISC transition with the strongest SOC is energetically downhill, where the relevant triplet state is energetically lower than S1 by 0.74 eV (T1) and 0.28 eV (T3) eV for P and CH, respectively. In the case of BC, we find an uphill process of 0.10 eV. The reorganization energies, λ , are calculated using Huang-Rhys factors (HRFs) based on the S1 and Tn optimized geometries and are found to be within 0.03 eV of the values obtained by direct calculation (i.e., using the energy difference of S1 [or Tn between the optimized excited singlet and the triplet geometries) confirming the harmonic approximation, see the Supporting Information, Table S5.

Overall the calculated SOCs are quite substantial, increasing with the degree of hydrogenation, with 0.48 cm⁻¹ for P, 0.68 cm⁻¹ for CH, and 1.09 cm⁻¹ for BC (see Table 2). We next turn to consider more closely the trend of the SOC that increases within the series upon hydrogenation. This trend results primarily from the electronic structure of the ring systems, whereas molecular structure changes do not impact the SOC significantly. To confirm this relationship, we recalculate the SOC after adding (removing) hydrogens without reoptimizing the ring structures.

The lowest SOC is found for P with 0.48 cm⁻¹, where for the doubly hydrogenated case it increases to 1.09 cm⁻¹. For example adding two pairs of hydrogens to P (while freezing the structure) results in a SOC of 1.00 cm⁻¹ that compares well with 1.09 cm⁻¹ of the BC system. Similarly removing the four hydrogens from BC results in a SOC of 0.37 cm⁻¹ that compares well with the SOC of P of 0.48 cm⁻¹.

To understand the SOC trend, we consider the detachment and attachment densities of S1 and the relevant Tn states in Figure 5. These densities underlie the nature of the excited state, whose density is obtained by removing the detachment

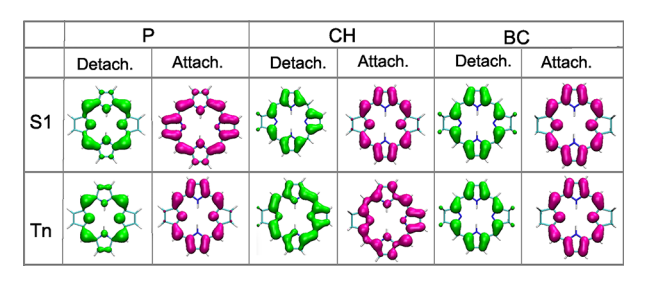


Figure 5. Detachment and attachment densities of S1 state and the relevant triplet state (T1 for P and T3 for CH and BC) at the S1-optimized geometry.

density from the ground state, and replacing it by the attachment density. The S1 detachment densities are similar to those of the relevant triplet state for all three molecules, whereas the attachment densities show increased overlap across the series, explaining the trend of the increasing SOC with that of P being the smallest. In the case of BC of the highest SOC, the singlet and triplet attachment densities are most similar, whereas they are different for CH and differ even further in the case of P relating the smallest SOC to the decreased overlap. We point out that the T3 in the case of P (T3 states are considered for BC and CH while T1 is considered for P) shows variance also in the detachment density resulting with an even smaller SOC of 0.05 cm⁻¹ compared to the 0.48 cm⁻¹ for the T1. (Additional densities for P are provided in the Supporting Information, Figure S2.)

This trend appears to result from differences between the S1 states where the triplet states are dominated by a single transition at the S1 geometry. The orbital transitions and coefficients of the relevant states at the S1-optimized geometry are detailed in Figure 4. (A more complete listing of the orbital energies and transitions is provided in the Supporting Information, Table S2.) The main transition for T1 of P has a coefficient of 0.89, where T3 in BC and CH bear a largest coefficient of 0.97. The S1 in P involves two close to equivalent orbital transitions reflecting the HOMO and HOMO-1 degeneracy. In CH and BC, where the orbital degeneracy is lifted, there is a dominant transition in S1 with a largest coefficient of 0.85 and 0.92, respectively. The lifting of orbital degeneracy and therefore change of the S1 state character leads to the increase of the overlap and therefore of the SOC trend to increase from P to CH and BC upon hydrogenation.

Next, we compare calculated ISC rates at the semiclassical and FGR levels. The largest ISC transition rate constants are presented in Table 3, where the other rates involving the three lowest triplet states are included in the Supporting Information, Table S6. We note that the second largest rate is significantly smaller (it is 4 orders of magnitude smaller in

the cases of P and CH). The calculated FGR rate constants are within the order of magnitude of the measured trends, where the ISC rate is the largest for BC. We point out that the measured values in toluene and those in the more polar solvent dimethylformamide (DMF) with a static dielectric constant of $\epsilon=38$ are very similar. In contrast to the fully quantum mechanical FGR theory, the semiclassical Marcus theory fails to accurately predict the rate constants, $k_{\rm ISC}$, especially for the P system. This trend is expected to occur in the inverted regime $\Delta E \gg \lambda$, where tunneling effects arise, that requires the fully quantum mechanical framework of the FGR approach.

We note that earlier studies on related systems find SOC values that are substantially smaller than those obtained by our calculations. 44,65 Accordingly and in spite of the rigidity of these systems several studies suggest that a non-Franck-Condon (FC) correction is important to reproduce the experimental ISC rate. 66,71,72 In particular, a corrected rate constant of 7.0×10^6 that compares well with the experimental measurement was recently reported, 71 whereas the uncorrected ISC rate was only at $3.0 \times 10^{2.66}$ However, we conjure that this indicated need for FC corrections to find large ISC rate constant depends on the level of the electronic structure. In fact, the finding reported in this paper that is based on the polarization-consistent electronic structure SRSH-PCM framework confirms the expectation that relatively rigid molecular systems as presented by the tetrapyrrolic rings can show only minor non-Condon effects. ^{73,74} See Supporting Information, Table S3, for SOC values at different geometries. We also point out that the increased rates reported above do not depend on the HRFs as suggested in earlier studies. 60 (Namely, while the HRFs found in our study are indeed larger than reported in ref 66 the rate constant remains larger also in the case where the HRFs are reset to the smaller values reported earlier.) For completeness, see HRF distributions shown in the Supporting Information, Figure S3.

Finally, we compare the ISC rate constants to the ones of the competing fluorescence process. The rate constants $k_{\rm f}$ in different systems are calculated based on the OSs, which are obtained using SRSH and listed in Table 1 and are included in Table 3. The calculated fluorescence rates are approximately of the same order of magnitude as the ones experimentally observed, where P shows the slowest rate. This is traced back, as explained above, to the quasi-degeneracy of the orbitals in P, leading to a near cancellation of the OS of the lowest excited state. ^{24,69,70} Importantly, we find that while the trends find that both $k_{\rm f}$ and $k_{\rm isc}$ are the slowest for P, the increase is by about 3 orders of magnitude for $k_{\rm isc}$ from P to BC, while the trend is much weaker for $k_{\rm f}$ of an increase by less than 1 order of magnitude. These trends are in good agreement with reported experimental values. ^{2,14,75}

Table 3. Calculated ISC Rate Constants Based on the Fully Quantum-Mechanical FGR Approach with a Damping Constant of 12.5 fs, $k_{\rm ISC}^{\rm FGR}$, and the Semi-Classical Marcus Theory, $k_{\rm ISC}^{\rm M}$, and Fluorescence Rate Constants $k_{\rm f}$ in Toluene^a

		intersystem crossing $k_{\rm ISC}$ (s ⁻¹)				fluorescence k_{f} (s $^{-1}$)			
		exp	o. ^b			exp.*			
molecule	transition			$k_{ m ISC}^{ m M}$	$k_{ m ISC}^{ m FGR}$			calc.	
P	$S1 \rightarrow T1$	5.9×10^{7} ¹⁴	(6.2×10^7)	1.6×10^{-12}	6.2×10^{7}	3.1×10^{6} ¹⁴	(5.5×10^6)	1.6×10^{5}	
CH	$S1 \rightarrow T3$		(9.1×10^7)	1.5×10^4	9.1×10^{7}	2.2×10^{7} ²²	(2.4×10^7)	9.7×10^{7}	
BC	$S1 \rightarrow T3$	1.5×10^{8} 15	(1.1×10^8)	2.0×10^{7}	1.1×10^{8}	$3.3 \times 10^{7.15}$	(4.0×10^7)	2.4×10^{8}	

^aFor completeness, the rates for other transitions are provided in the Supporting Information, Table S6. ^bMeasured $k_{\rm ISC}$ and $k_{\rm f}$ are of unsubstituted macrocycles in toluene. Rates in PEGylated macrocycles in DMF¹³ are noted in parentheses.

CONCLUSIONS

In conclusion, we have studied the trend of photophysical properties of tetrapyrrolic molecules as affected by the degree of ring conjugation using SRSH-PCM calculations. The calculated excited states are compared against measured spectral trends where the excitation energy is red-shifted and of increased oscillator strength in the P < CH < BC series. Indeed the fluorescence rate is found to increase in the series. The electronic excited states are then used to obtain the FGR and Marcus rate constants for the ISC. The FGR rates are in good agreement with measured values where the enhanced ISC rates in the series of P < CH < BC is due to increased SOC. Nonetheless, the ISC process appears to be the dominant process in the case of P due to the significantly decreased fluorescence rate. Lastly, we find that the fully quantum-mechanical FGR rate theory is essential for describing the $k_{\rm ISC}$ trend, especially in the cases of P and CH molecules that fall into the far-inverted regime.

ASSOCIATED CONTENT

Supporting Information

The Supporting Information is available free of charge at https://pubs.acs.org/doi/10.1021/acs.jpcc.1c03696.

Orbital energies and the transitions of S1 and Tn states at ground state and respective excited state geometries, reorganization energies (λ) in eV calculated using HRFs and direct methods, HRFs of the three molecules, and the xyz coordinates of all three molecules (PDF)

AUTHOR INFORMATION

Corresponding Author

Barry D. Dunietz – Department of Chemistry and Biochemistry, Kent State University, Kent, Ohio 44242, United States; oorcid.org/0000-0002-6982-8995; Email: bdunietz@kent.edu

Authors

Srijana Bhandari — Department of Chemistry and Biochemistry, Kent State University, Kent, Ohio 44242, United States; Present Address: Department of Chemistry, Case Western Reserve University, Cleveland, Ohio 44106, United States.

Sunandan Sarkar — Department of Chemistry and Biochemistry, Kent State University, Kent, Ohio 44242, United States; Present Address: Department of Chemistry, National Institute of Technology, Tiruchirappalli, Tamil Nadu 620015, India.

Alexander Schubert — Department of Chemistry and Biochemistry, Kent State University, Kent, Ohio 44242, United States; Department of Chemistry, University of Michigan, Ann Arbor, Michigan 48109, United States; Present Address: Institute of Physical Chemistry, Friedrich Schiller University Jena, 07743 Jena, Germany.; orcid.org/0000-0002-8560-6436

Atsushi Yamada – Department of Chemistry and Biochemistry, Kent State University, Kent, Ohio 44242, United States

Jameson Payne — Department of Chemistry and Biochemistry, Kent State University, Kent, Ohio 44242, United States Marcin Ptaszek — Department of Chemistry and Biochemistry, University of Maryland, Baltimore, Maryland 21250, United States; ⊚ orcid.org/0000-0001-6468-6900 Eitan Geva — Department of Chemistry, University of Michigan, Ann Arbor, Michigan 48109, United States; orcid.org/0000-0002-7935-4586

Complete contact information is available at: https://pubs.acs.org/10.1021/acs.jpcc.1c03696

Notes

The authors declare no competing financial interest.

ACKNOWLEDGMENTS

B.D.D. and E.G. would like to acknowledge support for this project by the Department of Energy (DOE), Basic Energy Sciences, through the Chemical Sciences Geosciences and Biosciences Division, through Grant No. DE-SC0016501. E.G. is grateful for support from the NSF via Grant No. CHE-1800325. A.S. is grateful for support from an ICAM fellowship, awarded by Kent State University and University of Michigan ICAM branches. We are also grateful to generous resource allocations on the Ohio Supercomputer Center⁷⁶ and the Kent State University, College of Arts and Sciences Computing Cluster.

REFERENCES

- (1) Zhao, J.; Wu, W.; Sun, J.; Guo, S. Triplet Photosensitizers: From Molecular Design to Applications. *Chem. Soc. Rev.* **2013**, 42, 5323–5351.
- (2) Arnaut, L. G. Design of porphyrin-based photosensitizers for photodynamic therapy. *Adv. Inorg. Chem.* **2011**, *63*, 187–233.
- (3) Xiang, H.; Cheng, J.; Ma, X.; Zhou, X.; Chruma, J. J. Near-infrared Phosphorescence: Materials and Applications. *Chem. Soc. Rev.* **2013**, *42*, 6128–6185.
- (4) Zhou, J.; Liu, Q.; Feng, W.; Sun, Y.; Li, F. Upconversion Luminescent Materials: Advances and Applications. *Chem. Rev.* **2015**, 115, 395–465.
- (5) Turro, N. J.; Ramamurthy, V.; Scaiano, J. C. Modern Molecular Photochemistry of Organic Molecules; University Science Books: Sausalito, CA, 2010.
- (6) Ji, S.; Ge, J.; Escudero, D.; Wang, Z.; Zhao, J.; Jacquemin, D. Molecular Structure–Intersystem Crossing Relationship of Heavy-Atom-Free BODIPY Triplet Photosensitizers. *J. Org. Chem.* **2015**, *80*, 5958–5963.
- (7) Zhao, J.; Chen, K.; Hou, Y.; Che, Y.; Liu, L.; Jia, D. Recent Progress in Heavy Atom-Free Organic Compounds Showing Unexpected Intersystem Crossing (ISC) Ability. *Org. Biomol. Chem.* **2018**, *16*, 3692–3701.
- (8) Klessinger, M. Triplet photoreactions; Structural dependence of spin-orbit coupling and intersystem crossing in organic biradicals. *Theor. Comput. Chem.* **1998**, *5*, 581–610.
- (9) Li, E. Y.-T.; Jiang, T.-Y.; Chi, Y.; Chou, P.-T. Semi-Quantitative Assessment of the Intersystem Crossing Rate: An Extension of the El-Sayed Rule to the Emissive Transition Metal Complexes. *Phys. Chem. Chem. Phys.* **2014**, *16*, 26184–26192.
- (10) Marian, C. M. Spin-orbit Coupling and Intersystem Crossing in Molecules. WIREs Comput. Mol. Sci. 2012, 2, 187–203.
- (11) Sarkar, S.; Hendrickson, H. P.; Lee, D.; Devine, F.; Jung, J.; Geva, E.; Kim, J.; Dunietz, B. D. Phosphorescence in Bromobenzal-dehyde Can. Be Enhanced through Intramolecular Heavy Atom Effect. J. Phys. Chem. C 2017, 121, 3771–3777.
- (12) Drzewiecka-Matuszek, A.; Skalna, A.; Karocki, A.; Stochel, G.; Fiedor, L. Effects of Heavy Central Metal on the Ground and Excited States of Chlorophyll. *JBIC, J. Biol. Inorg. Chem.* **2005**, *10*, 453–462. (13) Mandal, A. K.; Sahin, T.; Liu, M.; Lindsey, J. S.; Bocian, D. F.; Holten, D. Photophysical Comparisons of PEGylated Porphyrins, Chlorins and Bacteriochlorins in Water. *New J. Chem.* **2016**, *40*,

9648-9656.

- (14) Mandal, A. K.; Taniguchi, M.; Diers, J. R.; Niedzwiedzki, D. M.; Kirmaier, C.; Lindsey, J. S.; Bocian, D. F.; Holten, D. Photophysical Properties and Electronic Structure of Porphyrins Bearing Zero to Four Meso-Phenyl Substituents: New Insights into Seemingly Well Understood Tetrapyrroles. J. Phys. Chem. A 2016, 120, 9719—9731.
- (15) Yang, E.; Kirmaier, C.; Krayer, M.; Taniguchi, M.; Kim, H.-J.; Diers, J. R.; Bocian, D. F.; Lindsey, J. S.; Holten, D. Photophysical Properties and Electronic Structure of Stable, Tunable Synthetic Bacteriochlorins: Extending the Features of Native Photosynthetic Pigments. J. Phys. Chem. B 2011, 115, 10801–10816.
- (16) Harada, T.; Sano, K.; Sato, K.; Watanabe, R.; Yu, Z.; Hanaoka, H.; Nakajima, T.; Choyke, P. L.; Ptaszek, M.; Kobayashi, H. Activatable Organic Near-Infrared Fluorescent Probes Based on a Bacteriochlorin Platform: Synthesis and Multicolor in vivo Imaging with a Single Excitation. *Bioconjugate Chem.* **2014**, *25*, 362–369.
- (17) Alexander, V. M.; Sano, K.; Yu, Z.; Nakajima, T.; Choyke, P. L.; Ptaszek, M.; Kobayashi, H. Galactosyl Human Serum Albumin-NMP1 Conjugate: A Near Infrared (NIR)-Activatable Fluorescence Imaging Agent to Detect Peritoneal Ovarian Cancer Metastases. *Bioconjugate Chem.* **2012**, 23, 1671–1679.
- (18) Liu, T. W. B.; Chen, J.; Burgess, L.; Cao, W.; Shi, J.; Wilson, B. C.; Zheng, G. Multimodal Bacteriochlorophyll Theranostic Agent. *Theranostics* **2011**, *1*, 354.
- (19) Lovell, J. F.; Jin, C. S.; Huynh, E.; Jin, H.; Kim, C.; Rubinstein, J. L.; Chan, W. C. W.; Cao, W.; Wang, L. V.; Zheng, G. Porphysome Nanovesicles Generated by Porphyrin Bilayers for Use as Multimodal Biophotonic Contrast Agents. *Nat. Mater.* **2011**, *10*, 324.
- (20) Dogutan, D. K.; Ptaszek, M.; Lindsey, J. S. Direct Synthesis of Magnesium Porphine via 1-formyldipyrromethane. *J. Org. Chem.* **2007**, 72, 5008–5011.
- (21) Laha, J. K.; Muthiah, C.; Taniguchi, M.; McDowell, B. E.; Ptaszek, M.; Lindsey, J. S. Synthetic Chlorins Bearing Auxochromes at the 3-and 13-Positions. *J. Org. Chem.* **2006**, *71*, 4092–4102.
- (22) Kee, H. L.; Kirmaier, C.; Tang, Q.; Diers, J. R.; Muthiah, C.; Taniguchi, M.; Laha, J. K.; Ptaszek, M.; Lindsey, J. S.; Bocian, D. F.; et al. Effects of Substituents on Synthetic Analogs of Chlorophylls. Part 2: Redox Properties, Optical Spectra and Electronic Structure. *Photochem. Photobiol.* **2007**, *83*, 1125–1143.
- (23) Borbas, K. E.; Chandrashaker, V.; Muthiah, C.; Kee, H. L.; Holten, D.; Lindsey, J. S. Design, Synthesis, and Photophysical Characterization of Water-Soluble Chlorins. *J. Org. Chem.* **2008**, 73, 3145–3158.
- (24) Gouterman, M.; Wagnière, G. H.; Snyder, L. C. Spectra of Porphyrins: Part II. Four Orbital Model. *J. Mol. Spectrosc.* **1963**, *11*, 108–127
- (25) Hartzler, D. A.; Niedzwiedzki, D. M.; Bryant, D. A.; Blankenship, R. E.; Pushkar, Y.; Savikhin, S. Triplet Excited State Energies and Phosphorescence Spectra of (Bacterio) Chlorophylls. *J. Phys. Chem. B* **2014**, *118*, 7221–7232.
- (26) Yang, E.; Diers, J. R.; Huang, Y.-Y.; Hamblin, M. R.; Lindsey, J. S.; Bocian, D. F.; Holten, D. Molecular Electronic Tuning of Photosensitizers to Enhance Photodynamic Therapy: Synthetic Dicyanobacteriochlorins as a Case Study. *Photochem. Photobiol.* **2013**, *89*, 605–618.
- (27) Lindsey, J. S.; Mass, O.; Chen, C.-Y. Tapping the Near-Infrared Spectral Region with Bacteriochlorin Arrays. *New J. Chem.* **2011**, *35*, 511–516.
- (28) Lindsey, J. S. De novo Synthesis of Gem-Dialkyl Chlorophyll Analogues for Probing and Emulating our Green World. *Chem. Rev.* **2015**, *115*, 6534–6620.
- (29) Gouterman, M. In *The Porphyrins*; Dolphin, D., Ed.; Academic Press, 1978; Chapter 1, pp 1–165.
- (30) von Bünau, G. Buchbesprechung J. B. Birks: Photophysics of Aromatic Molecules. Wiley-Interscience, London 1970. 704 Seiten. Preis: 210s. Berichte der Bunsengesellschaft für Physikalische Chemie 1970, 74, 1294–1295.
- (31) Strickler, S.; Berg, R. A. Relationship between Absorption Intensity and Fluorescence Lifetime of Molecules. *J. Chem. Phys.* **1962**, *37*, 814–822.

- (32) Minaev, B.; Ågren, H. Theoretical DFT Study of Phosphorescence from Porphyrins. *Chem. Phys.* **2005**, 315, 215–239.
- (33) Redmond, R. W.; Gamlin, J. N. A Compilation of Singlet Oxygen Yields from Biologically Relevant Molecules. *Photochem. Photobiol.* **1999**, *70*, 391–475.
- (34) Bhandari, S.; Cheung, M.; Geva, E.; Kronik, L.; Dunietz, B. D. Fundamental Gaps of Condensed-Phase Organic Semiconductors From Single-Molecule Polarization-Consistent Optimally Tuned Screened Range-Separated Hybrid Functionals. *J. Chem. Theory Comput.* 2018, 14, 6287–6294.
- (35) Bhandari, S.; Dunietz, B. D. Quantitative Accuracy in Calculating Charge Transfer State Energies in Solvated Molecular Dimers Using Screened Range Separated Hybrid Functional Within a Polarized Continuum Model. J. Chem. Theory Comput. 2019, 15, 4305
- (36) Begam, K.; Bhandari, S.; Maiti, B.; Dunietz, B. D. Screened Range-Separated Hybrid Functional with Polarizable Continuum Model Overcomes Challenges in Describing Triplet Excitations in the Condensed Phase Using TDDFT. J. Chem. Theory Comput. 2020, 16, 3287.
- (37) Aksu, H.; Schubert, A.; Geva, E.; Dunietz, B. D. Explaining Spectral Asymmetries and Excitonic Characters of the Core Pigment Pairs in the Bacterial Reaction Center Using Screened Range-Separated Hybrid Functionals. *J. Phys. Chem. B* **2019**, *123*, 8970–8975.
- (38) Song, Y.; Schubert, A.; Maret, E.; Burdick, R. K.; Dunietz, B. D.; Geva, E.; Ogilvie, J. P. Vibronic Structure of Photosynthetic Pigments Probed by Polarized Two-dimensional Electronic Spectroscopy and ab initio Calculations. *Chem. Sci.* **2019**, *10*, 8143–8153.
- (39) Aksu, H.; Schubert, A.; Bhandari, S.; Yamada, A.; Geva, E.; Dunietz, B. D. On the Role of the Special Pair in Photosystems as a Charge Transfer Rectifier. *J. Phys. Chem. B* **2020**, *124*, 1987–1994.
- (40) Lee, M. H.; Geva, E.; Dunietz, B. D. Calculation from First-Principles of Golden Rule Rate Constants for Photoinduced Subphthalocyanine/Fullerene Interfacial Charge Transfer and Recombination in Organic Photovoltaic Cells. *J. Phys. Chem. C* **2014**, 118, 9780–9789.
- (41) Lee, M. H.; Dunietz, B. D.; Geva, E. Donor-to-Donor vs Donor-to-Acceptor Interfacial Charge Transfer States in the Phthalocyanine—Fullerene Organic Photovoltaic System. *J. Phys. Chem. Lett.* **2014**, *5*, 3810–3816.
- (42) Manna, A. K.; Dunietz, B. D. Communication: Charge-Transfer Rate Constants in Zinc-Porphyrin-Porphyrin-Derived Dyads: A Fermi Golden Rule First-Principles-Based Study. *J. Chem. Phys.* **2014**, *141*, 121102.
- (43) Lee, M. H.; Geva, E.; Dunietz, B. D. The Effect of Interfacial Geometry on Charge-Transfer States in the Phthalocyanine/Fullerene Organic Photovoltaic System. *J. Phys. Chem. A* **2016**, *120*, 2970–2975.
- (44) Etinski, M.; Tatchen, J.; Marian, C. M. Time-Dependent Approaches for the Calculation of Intersystem Crossing Rates. *J. Chem. Phys.* **2011**, *134*, 154105.
- (45) Rohrdanz, M. A.; Martins, K. M.; Herbert, J. M. A Long-Range-Corrected Density Functional That Performs Well for Both Ground-State Properties and Time-Dependent Density Functional Theory Excitation Energies, Including Charge-Transfer Excited States. *J. Chem. Phys.* **2009**, *130*, 054112–054119.
- (46) Perdew, J. P.; Burke, K.; Ernzerhof, M. Generalized Gradient Approximation Made Simple. *Phys. Rev. Lett.* **1996**, *77*, 3865.
- (47) Stein, T.; Kronik, L.; Baer, R. Prediction of Charge-Transfer Excitations in Coumarin-Based Dyes Using a Range-Separated Functional Tuned From First Principles. *J. Chem. Phys.* **2009**, *131*, 244119.
- (48) Lange, A. W.; Herbert, J. M. A Smooth, Nonsingular, and Faithful Discretization Scheme for Polarizable Continuum Models: The Switching/Gaussian Approach. J. Chem. Phys. 2010, 133, 244111.
- (49) Mewes, J.-M.; You, Z.-Q.; Wormit, M.; Kriesche, T.; Herbert, J. M.; Dreuw, A. Experimental Benchmark Data and Systematic Evaluation of Two a Posteriori, Polarizable-Continuum Corrections

- for Vertical Excitation Energies in Solution. J. Phys. Chem. A 2015, 119, 5446-5464.
- (50) Amatore, C.; Pfluger, F. Mechanism of Oxidative Addition of Palladium (0) with Aromatic Iodides in Toluene, Monitored at Ultramicroelectrodes. *Organometallics* **1990**, *9*, 2276–2282.
- (51) Kedenburg, S.; Vieweg, M.; Gissibl, T.; Giessen, H. Linear Refractive Index and Absorption Measurements of Nonlinear Optical Liquids in the Visible and Near-Infrared Spectral Region. *Opt. Mater. Express* **2012**, *2*, 1588–1611.
- (52) Hirata, S.; Head-Gordon, M. Time-Dependent Density Functional Theory within the Tamm-Dancoff Approximation. *Chem. Phys. Lett.* **1999**, 314, 291–299.
- (53) Mussard, B.; Sharma, S. One-Step Treatment of Spin-Orbit Coupling and Electron Correlation in Large Active Spaces. *J. Chem. Theory Comput.* **2018**, *14*, 154–165.
- (54) Shao, Y.; Gan, Z.; Epifanovsky, E.; Gilbert, A. T. B.; Wormit, M.; Kussmann, J.; Lange, A. W.; Behn, A.; Deng, J.; Feng, X.; et al. Advances in Molecular Quantum Chemistry Contained in the Q-Chem 4 Program Package. *Mol. Phys.* **2015**, *113*, 184–215.
- (55) Frisch, M. J.; Trucks, G. W.; Schlegel, H. B.; Scuseria, G. E.; Robb, M. A.; Cheeseman, J. R.; Scalmani, G.; Barone, V.; Mennucci, B.; Petersson, G. A.; et al., *Gaussian 09*, Rev. A.02; Gaussian Inc.: Wallingford, CT, 2016.
- (56) Nitzan, A. Chemical Dynamics in Condensed Phases: Relaxation, Transfer and Reactions in Condensed Molecular Systems: Relaxation, Transfer and Reactions in Condensed Molecular Systems; Oxford University Press: 2006.
- (57) Kee, H. L.; Diers, J. R.; Ptaszek, M.; Muthiah, C.; Fan, D.; Lindsey, J. S.; Bocian, D. F.; Holten, D. Chlorin—Bacteriochlorin Energy-transfer Dyads as Prototypes for Near-infrared Molecular Imaging Probes: Controlling Charge-Transfer and Fluorescence Properties in Polar Media. *Photochem. Photobiol.* **2009**, 85, 909—920.
- (58) Marcus, R. A. On the Theory of Oxidation-Reduction Reactions Involving Electron Transfer. I. *J. Chem. Phys.* **1956**, 24, 966–978.
- (59) Marcus, R. A. Electrostatic Free Energy and Other Properties of States Having Nonequilibrium Polarization. I. *J. Chem. Phys.* **1956**, 24, 979–989.
- (60) Marcus, R. A.; Sutin, N. Electron Transfers in Chemistry and Biology. *Biochim. Biophys. Acta, Rev. Bioenerg.* 1985, 811, 265–322.
- (61) Marcus, R. A. Electron Transfer Reactions in Chemistry. Theory and Experiment. *Rev. Mod. Phys.* **1993**, *65*, 599–610.
- (62) Sarkar, S.; Protasiewicz, J. D.; Dunietz, B. D. Controlling the Emissive Activity in Heterocyclic Systems Bearing C = P Bonds. *J. Phys. Chem. Lett.* **2018**, *9*, 3567–3572.
- (63) Nguyen, K. A.; Day, P. N.; Pachter, R.; Tretiak, S.; Chernyak, V.; Mukamel, S. Analysis of Absorption Spectra of Zinc Porphyrin, Zinc m eso-Tetraphenylporphyrin, and Halogenated Derivatives. *J. Phys. Chem. A* **2002**, *106*, 10285–10293.
- (64) Nemykin, V. N.; Hadt, R. G.; Belosludov, R. V.; Mizuseki, H.; Kawazoe, Y. Influence of Molecular Geometry, Exchange-Correlation Functional, and Solvent Effects in the Modeling of Vertical Excitation Energies in Phthalocyanines using Time-Dependent Density Functional Theory (TDDFT) and Polarized Continuum Model TDDFT Methods: Can Modern Computational Chemistry Methods Explain Experimental Controversies? *J. Phys. Chem. A* **2007**, *111*, 12901–12913.
- (65) Perun, S.; Tatchen, J.; Marian, C. M. Singlet and Triplet Excited States and Intersystem Crossing in Free-Base Porphyrin: TDDFT and DFT/MRCI Study. *ChemPhysChem* **2008**, *9*, 282–292.
- (66) Valiev, R. R.; Cherepanov, V. N.; Baryshnikov, G. V.; Sundholm, D. First-Principles Method for Calculating the Rate Constants of Internal-Conversion and Intersystem-Crossing Transitions. *Phys. Chem. Chem. Phys.* **2018**, 20, 6121–6133.
- (67) Mewes, S. A.; Plasser, F.; Krylov, A.; Dreuw, A. Benchmarking Excited-State Calculations Using Exciton Properties. *J. Chem. Theory Comput.* **2018**, *14*, 710–725.

- (68) Konig, C.; Neugebauer, J. Quantum Chemical Description of Absorption Properties and Excited-State Processes in Photosynthetic Systems. *ChemPhysChem* **2012**, *13*, 386–425.
- (69) White, W.; Dolphin, D. The Porphyrins. Phys. Chem. C 1978, 493-501.
- (70) Hasegawa, J.; Ohkawa, K.; Nakatsuji, H. Excited States of the Photosynthetic Reaction Center of Rhodopseudomonas viridis: SACCI Study. *J. Phys. Chem. B* **1998**, *102*, 10410–10419.
- (71) Valiev, R. R.; Cherepanov, V. N.; Nasibullin, R. T.; Sundholm, D.; Kurten, T. Calculating Rate Constants for Intersystem Crossing and Internal Conversion in the Franck-Condon and Herzberg-Teller Approximations. *Phys. Chem. Chem. Phys.* **2019**, *21*, 18495–18500.
- (72) Santoro, F.; Lami, A.; Improta, R.; Bloino, J.; Barone, V. Effective Method for the Computation of Optical Spectra of Large Molecules at Finite Temperature Including the Duschinsky and Herzberg—Teller Effect: The Qx Band of Porphyrin as a Case Study. *J. Chem. Phys.* **2008**, *128*, 224311.
- (73) Gentemann, S.; Medforth, C. J.; Forsyth, T. P.; Nurco, D. J.; Smith, K. M.; Fajer, J.; Holten, D. Photophysical Properties of Conformationally Distorted Metal-Free Porphyrins. Investigation into the Deactivation Mechanisms of the Lowest Excited Singlet State. J. Am. Chem. Soc. 1994, 116, 7363–7368.
- (74) Wasielewski, M. R.; Niemczyk, M. P.; Svec, W. A.; Pewitt, E. B. Dependence of Rate Constants for Photoinduced Charge Separation and Dark Charge Recombination on the Free energy of Reaction in Restricted-Distance Porphyrin-Quinone Molecules. *J. Am. Chem. Soc.* 1985, 107, 1080–1082.
- (75) Yang, E.; Kirmaier, C.; Krayer, M.; Taniguchi, M.; Kim, H.-J.; Diers, J. R.; Bocian, D. F.; Lindsey, J. S.; Holten, D. Photophysical Properties and Electronic Structure of Stable, Tunable Synthetic Bacteriochlorins: Extending the Features of Native Photosynthetic Pigments. J. Phys. Chem. B 2011, 115, 10801–10816.
- (76) Ohio Supercomputer Center; 1987; http://osc.edu/ark:/19495/f5s1ph73. Accessed on 01.01.2014.